Journal of Structural Biology 193 (2016) 124–131

Contents lists available at ScienceDirect

Journal of Structural Biology

journal homepage: www.elsevier.com/locate/yjsbi

Ordering of protein and water molecules at their interfaces with chitin nano-crystals

Clara Valverde Serrano [a], Hanna Leemreize [a], Benny Bar-On [b,a], Friedrich G. Barth [c], Peter Fratzl [a], Emil Zolotoyabko [d], Yael Politi [a,*]

[a] Department of Biomaterials, Max Planck Institute of Colloids and Interfaces, Research Campus Golm, 14424 Potsdam, Germany
[b] Department of Mechanical Engineering, Ben-Gurion University, Beer Sheba 84105, Israel
[c] Department of Neurobiology, Faculty of Life Sciences, University of Vienna, 1090 Vienna, Austria
[d] Department of Materials Science and Engineering, Technion-Israel Institute of Technology, Haifa 32000, Israel

ARTICLE INFO

Article history:
Received 27 October 2015
Received in revised form 8 December 2015
Accepted 11 December 2015
Available online 11 December 2015

Keywords:
Chitin
Chitin/protein interaction
Chitin/water interaction
X-ray diffraction

ABSTRACT

Synchrotron X-ray diffraction was applied to study the structure of biogenic α-chitin crystals composing the tendon of the spider *Cupiennius salei*. Measurements were carried out on pristine chitin crystals stabilized by proteins and water, as well as after their deproteinization and dehydration. We found substantial shifts (up to $\Delta q/q = 9\%$ in the wave vector in q-space) in the (020) diffraction peak position between intact and purified chitin samples. However, chitin lattice parameters extracted from the set of reflections (*hkl*), which did not contain the (020)-reflection, showed no systematic variation between the pristine and the processed samples. The observed shifts in the (020) peak position are discussed in terms of the ordering-induced modulation of the protein and water electron density near the surface of the ultra-thin chitin fibrils due to strong protein/chitin and water/chitin interactions. The extracted modulation periods can be used as a quantitative parameter characterizing the interaction length.

1. Introduction

Organisms produce a wide range of intricately structured biocomposites exhibiting hierarchical architectures at multiple length scales, from nanometers to millimeters. Vertebrate bones and teeth or mollusk shells are familiar examples, which are composites of biopolymers and minerals (Weiner and Wagner, 1998; Lowenstam and Weiner, 1989; Mann, 2001). On the other hand, plant materials such as wood are non-mineralized load-bearing biological composites comprised of polysaccharide fibers (cellulose) embedded in an amorphous polysaccharide (hemicellulose) and a complex aromatic alcohol polymer (lignin) matrix (Fengel and Wegener, 1984). Similar to wood, the spider cuticle, which is the subject of the current work, is a non-mineralized biomaterial built of semi-crystalline polysaccharide fibers (chitin) embedded into a hydrated protein matrix (Barth, 1973).

The interactions between the load-bearing components (polymeric fibers or minerals) and the (organic) matrix are of great importance to both the formation mechanisms and the mechanical performance of composite biological materials (Berman et al., 1988, 1990; Pokroy et al., 2004; Zolotoyabko and Pokroy, 2007). Importantly, the interaction of the organic molecules with specific atomic planes within biogenic calcium carbonate has been established (Berman et al., 1990; Pokroy et al., 2006a,b) and shown to induce anisotropic lattice distortions in the mineral. Distortions reach a maximum of about 0.2% along the c-axis in both biogenic aragonite and calcite and disappear upon mild annealing at 200–250 °C, which selectively destroys the organic matrix (Pokroy et al., 2004, 2006a,b).

The interactions between the proteins and the load-bearing chitin crystals in various arthropod cuticles have been studied using X-ray diffraction, biochemical methods, and molecular modeling. Early reports (Fraenkel and Rudall, 1947; Rudall, 1963) outlined the agreement between repeating distances along the c-axis in the orthorhombic chitin crystal structure (extracted from X-ray diffraction measurements) and the expected repeats along β-strands in pleated sheet motifs in specific matrix proteins, which would allow for multiple interactions between chitin and the proteins (Neville, 1993). Atkins (1985) identified another repeating distance of 0.475 nm, which is the spacing between chitin chains along the a-axis within the (010)-planes and also the distance between strands in a pleated protein β-sheet structure.

* Corresponding author.
E-mail address: yael.politi@mpikg.mpg.de (Y. Politi).

http://dx.doi.org/10.1016/j.jsb.2015.12.004
1047-8477/

In the arthropod cuticle, each chitin crystal is coated with globular proteins that give rise to additional features in the diffraction pattern of the cuticle, which is otherwise dominated by the diffraction from the chitin crystals. Blackwell and Weih (1980) showed the presence of axial layer-lines in the 2D X-ray diffraction pattern of the intact ovipositor cuticle of the wasp *Megarhyssa*, corresponding to a protein repeat of 3.06 nm along the chitin fibril and suggested that the protein consists of sub-units arranged in a 6_1-helix around the crystalline chitin core. It was also deduced that the protein/chitin interaction in the ovipositor of the wasp *Megarhyssa* takes place on the (0 1 0) chitin plane, presumably by multiple hydrogen bonds (Atkins, 1985; Blackwell and Weih, 1980; Vincent and Wegst, 2004; Neville, 1967).

Biochemical studies of proteins from a wide variety of arthropod cuticles identified a conserved chitin-binding sequence, the so-called R&R consensus sequence (Rebers and Willis, 2001). Using homology modeling, it was suggested that the preferred secondary structure of chitin binding domain in cuticular proteins, the so-called R&R consensus sequence, is an antiparallel β-sheet structure in a half β-barrel structure. In this configuration aromatic residues face the internal β-barrel surface and are expected to interact with the chitin crystals (Suetake et al., 2000; Iconomidou et al., 2005).

In this article, we shed additional light on the protein/chitin and water/chitin interactions, by studying X-ray diffraction profiles from biogenic chitin in its intact, deproteinized, hydrated and dried state. We model the protein- and water-induced modulation of the diffraction profiles, and track the apparent changes in the lattice parameter, *b*, upon dehydration and deproteinization. The investigated chitin crystals are the building blocks of the arthropod cuticle, specifically, the tarsal tendons of the wandering spider *Cupiennius salei*.

2. Materials and methods

2.1. Samples

Adult specimens of the Central American wandering spider *C. salei* (Barth, 2002) were obtained from the breeding stock at the Department of Neurobiology of the University of Vienna. The spiders were transported in dry ice and stored at −20 °C for 3 months at maximum. Tendons were pulled from the metatarsus segment of the leg and mechanically cleaned from muscle residues. The dorsal and the ventral tendons were indiscriminately used.

2.2. Partial and full deproteinization by basic treatment and bleaching

For partial deproteinization, tendons were immersed in 15 mL of 40% w/w KOH aqueous solution and heated at 70 °C under continuous stirring for 30 min. The samples were then thoroughly washed with distilled water and air-dried. The level of deproteinization was monitored by amino acid analysis (data not shown). Pure chitin – full deproteinization – was obtained by immersing tibiae cuticle samples in 0.3% NaClO solution buffered at pH 4.9 in 0.1 N acetate buffer solution at 70 °C for 3 h after an initial partial deproteinization treatment with KOH as described above.

2.3. Wide-angle X-ray scattering (WAXS)

Tendon samples attached to a silicon frame were mounted vertically in a custom-made humidity-controlled chamber and measured at a dedicated SAXS/WAXS station of the μ-Spot beam line at the synchrotron BESSY II (Helmholtz Center, Berlin, Germany). An X-ray energy of E_x = 15 keV (λ = 0.0826 nm) was chosen from the synchrotron radiation spectrum by a multilayered monochromator (bandwidth $\Delta E_x/E_x \approx 0.01$). The incident X-ray beam was focused on the sample by a toroidal mirror, and the final beam size was defined by a pinhole of 100 μm diameter placed in front of the sample. WAXS data were collected using a large-area 2D detector (MarMosaic 225, Mar USA Evanston, USA), situated approximately 300 mm behind the sample. The sample-to-detector distance was calibrated by measuring the diffraction from quartz standard.

Tendon and tibiae samples were measured at three different positions along the sample. For converting the 2D diffraction data into 1D profiles (as a function of the scattering vector, *q*), Matlab 8.6 software and the in-house SAXS/WAXS analysis software DPDAK (https://dpdak.desy.de/index.php/Hauptseite) were used. Selected diffraction profiles were fitted to pseudo-Voigt functions with a linear background using OriginPro9.1. For fitting peak positions, the scattering vector *q* was converted to *d*-spacing by applying Bragg's law ($d = 2\pi/q$). The extracted lattice parameters were determined using the peak positions of the (0 0 4), (0 4 2), (0 2 1), (1 1 0) and (0 1 3) reflections and averaged over the relevant measurement set.

2.4. Humidity control

A custom-made chamber was used to control temperature and humidity during X-ray measurements. The temperature was controlled using a thermostat (HUBER Ministat). The relative humidity (RH) was controlled using a WETSYS humidity generator (SETARAM) and was monitored by an EK-H4 Evaluation Kit (Sensirion) set up with a SHT75 capacitive sensor placed a few millimeters away from the sample. The accuracy of the RH and temperature readings was ±2% and ±0.5 °C, respectively. Humidity was set to a constant RH of 10% for "dry" samples and 90% for "wet" samples. All samples were equilibrated for one hour prior to diffraction measurements.

2.5. Raman spectroscopy

Spectra were acquired with a confocal Raman microscope (CRM200, Witec, Germany) equipped with a piezo scanner (P-500, Physik Instrumente, Karlsruhe, Germany). A linearly polarized near-infrared diode-laser (Toptica Photonics AG, Graefelfing, Germany) was used in combination with a Nikon 20× microscope lens. The spectra were acquired using an air-cooled CCD (PI-MAX, Princeton Instruments Inc., Trenton, NJ, USA) behind a grating (300 g/mm) spectrograph. The overall Raman intensity was maximized by adjusting the laser focus by means of an integrated light-microscope. The ScanCtrl Spectroscopy Plus software (Witec, Germany) was used for spectra acquisition (three hardware accumulations, ten software accumulations, 1 s integration time) and WiTec Project Plus was used for data processing.

3. Results and discussion

The tarsal tendon is used by the spider to flex its tarsus (the last segment of the leg) and to move the pretarsus containing the claws (Speck and Barth, 1982). The tendon is built of tightly packed α-chitin fibrils surrounded by proteins, which are aligned along the chitin *c*-axis (Fig. 1). The atomic structure of pure α-chitin was the subject of several comprehensive studies (Blackwell and Weih, 1980; Minke and Blackwell, 1978; Carlström, 1987; Sikorski et al., 2009). The space group is $P2_12_12_1$; and its orthorhombic unit cell has the following dimensions: a = 0.474 nm, b = 1.886 nm and c = 1.032 nm (Minke and Blackwell, 1978). The main motif of this structure comprises the adjacent polysaccharide chains running in antiparallel directions along the *c*-axis (crystallographic and fiber axis). The chains construct molec-

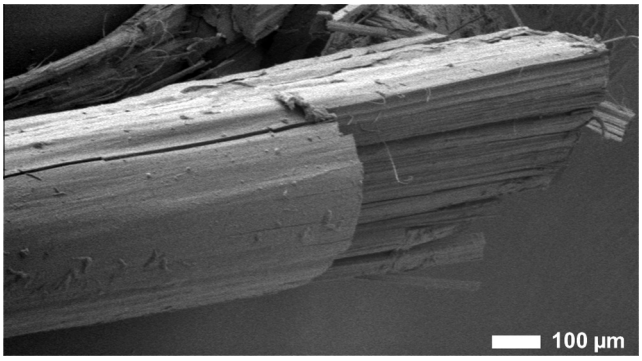

Fig. 1. Scanning electron microscopy (SEM) image of the cryo-fractured tendon revealing nearly parallel fiber arrangement.

ular sheets by forming hydrogen bonds nearly parallel to the *a*-axis, and the sheets are stacked along the *b*-axis by additional hydrogen bonding. Less attention, however, has been given to potential structural modifications due to the protein/chitin and water/chitin interactions in pristine (intact) samples.

In order to better understand these interactions within the tendons, we collected X-ray diffraction patterns from intact, partially- and fully-deproteinized tendon and tibia samples kept at low (dry) and high (wet) relative humidity. Details of sample preparation are given in the Section 2. The 2D diffraction diagrams of tendon specimens mounted vertically show the characteristic symmetry of the fiber diffraction pattern with reflections along the equatorial axis, originating in (*hk0*)-type chitin planes, and meridian reflections, originating in (*0 0 l*)-planes (Fig. 2A). Along the equatorial axis, the (020) and (110) reflections are most intense. Between these two reflections, additional low intensity reflections at angular positions corresponding to the scattering vectors $q = 9.44\ \mathrm{nm}^{-1}$ ($d = 2\pi/q = 6.66$ Å) and $q = 11.45\ \mathrm{nm}^{-1}$ ($d = 5.48$ Å), marked by arrowheads in Fig. 2B, are seen in intact, but not in partially deproteinized samples. These weak reflections correspond to those formerly observed in the ichneumonid wasp *Megarhyssa* species (Atkins, 1985; Blackwell and Weih, 1980) and attributed to subsidiary maxima in the four-chain thick chitin crystals (Atkins, 1985). Close to the meridian axis, four reflections are seen: the (001), (002), (012) reflections (the latter partially overlapping

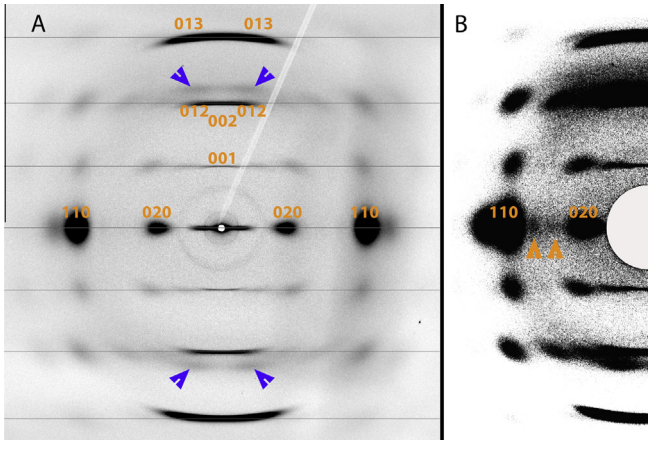

Fig. 2. (A) Typical diffraction pattern of an intact dry tendon, mounted with the chitin fibers oriented vertically. Layer lines and diffraction planes, as well as the diffraction spots resulting from the protein structure (blue arrow heads) are indexed. (B) High-contrast diffraction pattern of an intact tendon, revealing two additional intensity maxima (arrowheads) at $q = 9.44\ \mathrm{nm}^{-1}$ and $q = 11.45\ \mathrm{nm}^{-1}$ between the (110) and (020) diffraction spots.

with the (002)-reflection), and the (013) reflection (Fig. 2A). In α-chitin single crystals, the (012) and (013) vectors of the reciprocal lattice are inclined with respect to the [001]-axis by 15.3° and 10.3°, respectively. However, due to some angular spread of chitin fibrils about the main axis, the corresponding diffraction spots transform into arcs, which overlap along corresponding Debye–Scherrer rings. A rather intense reflection appears in intact samples close to the meridian, at $q = 13.82\ \mathrm{nm}^{-1}$ ($d = 4.54$ Å). This reflection does not correspond to an integer number of fiber layer-lines and disappears upon deproteinization (see Fig. 3A). For these reasons, we attribute it to the protein matrix. In fact, *d*-spacings in the range of 4.5–4.7 Å are characteristic for strand spacings in a pleated β-sheet motif (Merkel et al., 1999) and have been observed in X-ray diffraction patterns taken, for example, from silk (Valluzzi and Jin, 2004; Fossey and Kaplan, 1993; Geddes et al., 1968) and amyloid peptides (Sunde et al., 1997; Jahn et al., 2010). We use the disappearance of this reflection as evidence of a substantial decrease in the amount of proteins in our samples after the appropriate chemical treatment. The occurrence of the β-sheet motif within the protein matrix in intact tendon samples is also confirmed by Raman spectroscopy, which shows an intense peak at $1669\ \mathrm{cm}^{-1}$ characteristic of the protein β-sheet configuration (Iconomidou et al., 2001) (Fig. 4).

An important experimental finding emerges from comparing the diffraction patterns of bleached (i.e. fully deproteinized) and intact chitin samples (Fig. 5). In the bleached dry sample (with no proteins, measured at low relative humidity), the (020)-type diffraction spots and (021)-type diffraction spots have the same (010)-projection in reciprocal space (i.e. the same distance along the equatorial line in Fig. 5A). However, in the presence of proteins (Fig. 5B), the (020)-type and (021)-type diffraction spots possess clearly different (010)-projections along the equatorial line. The projection of the (020)-type diffraction spots in the intact sample is significantly shorter than that of the (021)-type diffraction spots. This implies that a *b*-lattice parameter value extracted from the (020)-reflection will be substantially larger than that extracted using the (021) or other (*hkl*) reflections.

In fact, with the exception of the (020) reflection, when analyzing all other reflections with sufficient intensity, we find no systematic differences in lattice parameters, *a*, *b*, and *c*, following processing. The obtained data for pristine, deproteinized, and bleached samples are summarized in Table 1 and compared with well-documented lattice parameters for pure chitin (Minke and Blackwell, 1978). Thus extracted lattice parameters deviate from tabulated values for pure chitin by less than 1% (Fig. 6).

When comparing the (020) diffraction profiles in pristine and treated chitin samples, we observe remarkable shifts in peak position, as is illustrated in Fig. 7A. Correspondingly, the lattice parameter *b*, extracted directly from the (020)-reflection, shows a large increase relative to the bleached dry state, reaching up to about 9% for intact wet and 6.5% for intact dry samples (see Fig. 7B). Even in deproteinized and bleached samples measured at high relative humidity (deproteinized wet and bleached wet, respectively), this increase is preserved at the level of 1.5%. The possible origin of these findings is considered below in Section 3.1.

Another interesting observation is the sharpening of the chitin diffraction spots after protein removal (see Fig. 3A). This effect is especially clear in the (020) diffraction profiles (Fig. 7A). The large broadening of the diffraction profiles in pristine chitin samples is expected since we know from transmission electron microscopy (TEM) measurements (Barth, 1973; Atkins, 1985; Neville and Parry, 1976; Erko et al., 2013) that the chitin fibril diameter (in the *b*-direction) is about 3–4 nm (i.e. two unit cells only). Narrowing of the diffraction profiles following protein removal is attributed to the coalescence of chitin crystallites. The coalescence is likely mediated by hydrogen bonds, which were previously satu-

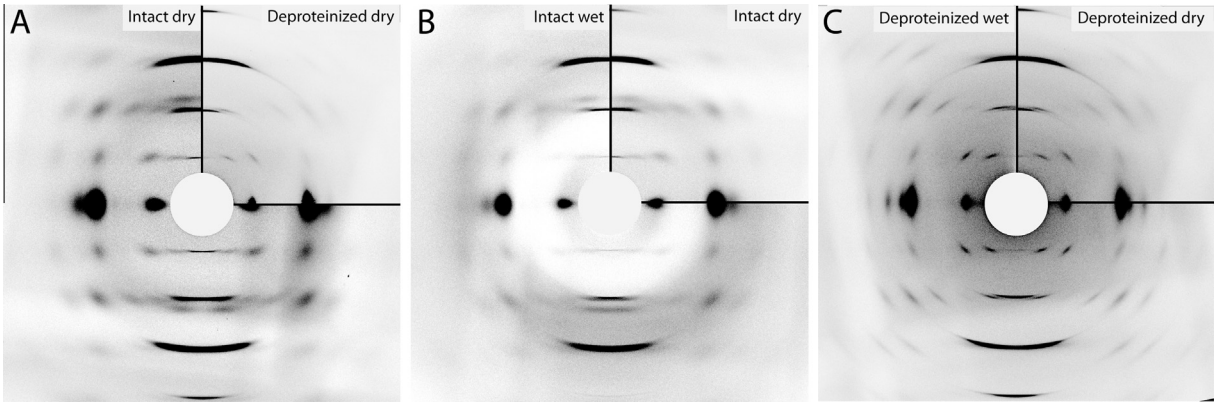

Fig. 3. Diffraction pattern of: (A) an intact tendon compared with a tendon deproteinized by chemical treatment (upper right corner insert); (B) an intact tendon – wet and dry (insert); (C) a tendon deproteinized by chemical treatment – wet and dry (insert).

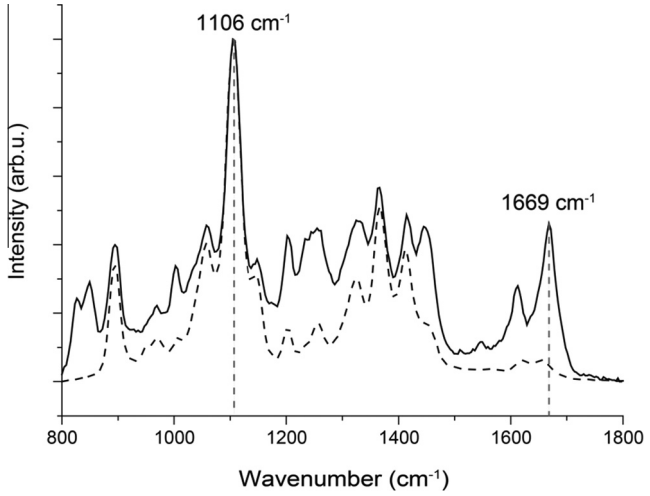

Fig. 4. Raman spectrum in the 800–1800 cm^{-1} region of a pristine (solid) and a deproteinized (dashed) tendon. The chitin peak at 1106 cm^{-1}, assigned to symmetric stretching of (COC), glycosidic bond, and the β sheet related peak at 1669 cm^{-1} are indicated.

rated by the interactions with the proteins. In the Section 3.1, we extract the sizes of chitin crystallites in the framework of the developed structural model. We note that the processing mentioned is not expected to interfere with the bulk of chitin structure itself, as confirmed by the X-ray diffraction patterns, or to cause

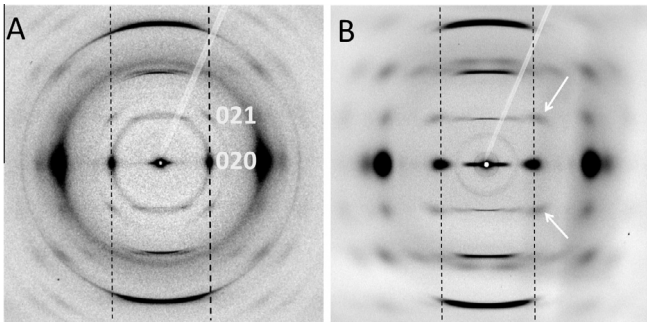

Fig. 5. (A) Diffraction pattern taken from a bleached (fully deproteinized) sample in dry state: vertical dashed lines cross the centers of the (020)-type diffraction spots; the (021)-type diffraction spots lie on the same vertical lines. (B) Diffraction pattern taken from an intact (with proteins) sample in dry state: the (021)-type diffraction spots, indicated by white arrows, are positioned away from vertical lines crossing the centers of the (020)-type diffraction spots.

Table 1
Lattice parameters, *a*, *b*, and *c*, extracted for intact and differently processed chitin samples, by using the set of X-ray reflections (*hkl*), excluding the (020)-reflection.

Sample	*a* (nm)	*b* (nm)	*c* (nm)
Intact wet	0.4739 ± 0.0005	1.884 ± 0.02	1.031 ± 0.005
Intact dry	0.470 ± 0.001	1.897 ± 0.013	1.028 ± 0.001
Deproteinized wet	0.477 ± 0.004	1.876 ± 0.011	1.035 ± 0.013
Deproteinized dry	0.474 ± 0.002	1.875 ± 0.019	1.032 ± 0.009
Bleached wet	0.477 ± 0.003	1.886 ± 0.011	1.032 ± 0.001
Bleached dry	0.474 ± 0.002	1.876 ± 0.012	1.032 ± 0.002
Minke and Blackwell (1978)	0.474 ± 0.001	1.886 ± 0.002	1.032 ± 0.002

significant deacetylation. The latter assumption was tested by Raman spectroscopy (Fig. 4), which shows the intense band at $\bar{\upsilon} = 1106\ cm^{-1}$ assigned to symmetric stretch of the C–O–C glycosidic bond (Zhang et al., 2012; Cheol Min et al., 2013) without any observable shift to higher wavenumbers associated with deacetylation (Zhang et al., 2012).

3.1. Model calculations

The forces acting between the protein/water and the chitin molecules may cause a modulation of the protein/water electron density close to their interface with chitin. This phenomenon is known to evolve at a monolayer scale in many two-phase systems (see e.g. Oh et al., 2005 and references therein). If the chitin crystal is very thin, the diffraction profile will be strongly influenced by the modulated electron density of the adjacent protein/water layer and the main diffraction peak will be shifted, erroneously imitating a change in lattice parameter. The largest effect of this type is indeed expected in the *b*-direction, along which the size of the intact chitin crystals is only about two unit cells. We also know that the (010) plane in chitin is a good candidate for strong interaction with proteins (Atkins, 1985) and water because of the availability of unsaturated hydrogen bonds in the *b*-direction.

Below, we calculate (in kinematic approximation) the modifications in X-ray diffraction profiles induced by such ordering processes in the proximity to the chitin surface. Specifically, we simulate the (020) diffraction profiles within a simple model, containing *N* chitin chains parallel to the *c*-axis. The chitin chains are sandwiched between two protein/water sub-layers (on both sides) with modulated electron density (Fig. 8A). In other words, we assume that the essential electron density modulation expands from the chitin interface up to two protein/water monolayers (as is found e.g. in Oh et al., 2005). The chitin chains are separated

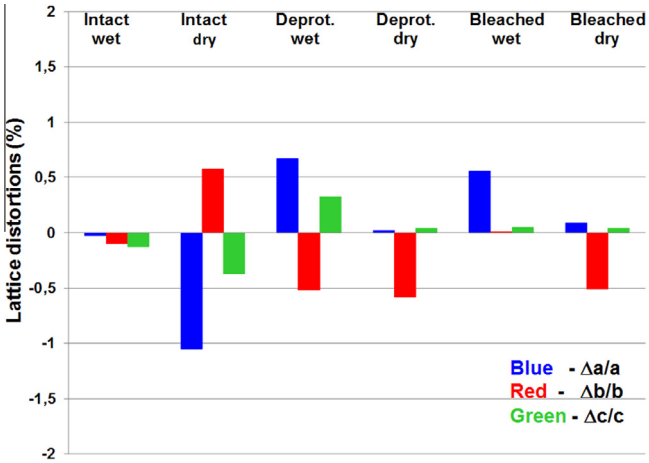

Fig. 6. Relative deviations of lattice parameters (in percent), measured in differently treated chitin samples, as compared with those in pure chitin (Minke and Blackwell, 1978). Reflection (020) is not considered.

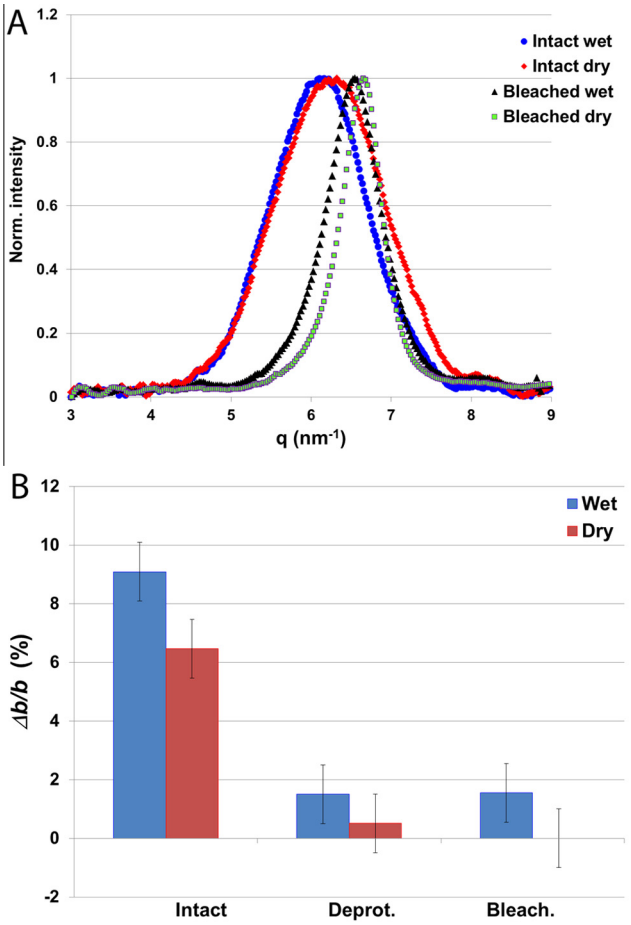

Fig. 7. (A) Normalized (020) diffraction profiles (after background subtraction), measured in intact and bleached chitin samples (wet and dried). (B) Apparent relative change of lattice parameter, b (in percent), in differently treated samples with respect to that in the bleached and dried chitin, as extracted from the (020) peak position.

by distance, $L = b/2$, whereas the protein/water modulation spacing is S.

In the case of coherent interfaces (with no stochastic phase jumps in scattered wave functions), the X-ray scattering

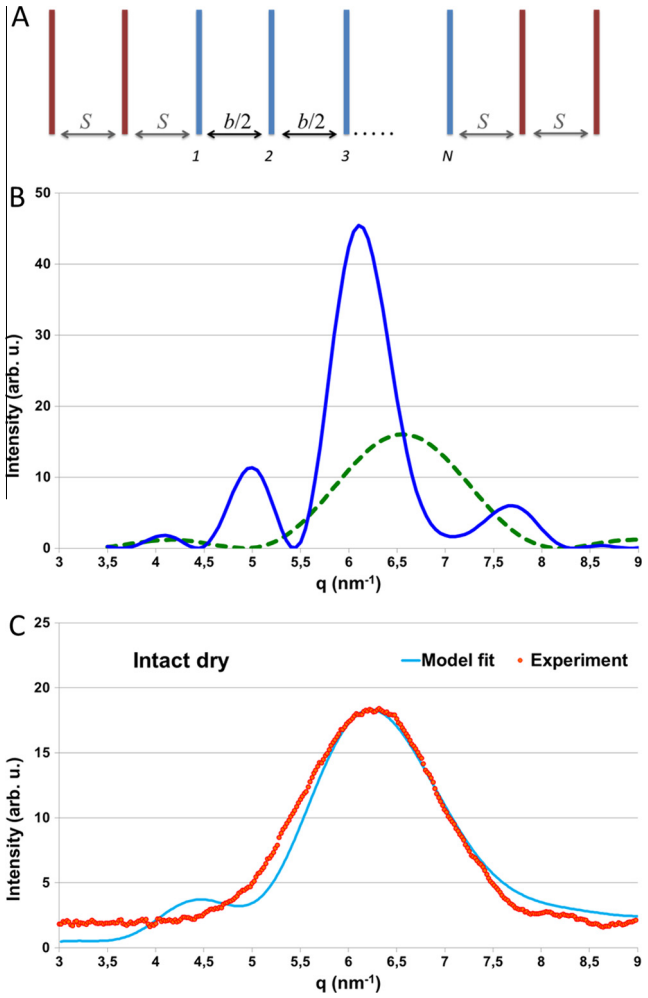

Fig. 8. (A) Schematic depiction of the chitin-protein cross-section along the b-axis denoting the diffraction model parameters. Blue lines represent chitin strands. Red lines represent protein layers. (B) Diffraction profiles, simulated by means of Eq. (2) (blue solid line) and Eq. (3) (green dashed line), showing strong effect of modulated protein electron density on the re-distribution of diffraction intensity in reciprocal space. Parameter $S = 1.13$ nm and $N = 4$. (C) The (020) diffraction profile, measured in the intact dry sample (orange dots), after polynomial background subtraction, superimposed on the simulated one (light-blue solid line) using Eqs. (6)–(9): $b = 1.89$ nm, $N = 3$, $S = 1.09$ nm, $\sigma = 0.19$ nm.

amplitude, F, generated by such a structure, is described by the following equation (as a function of the scattering vector, q):

$$F(q) = f_1(1 + e^{iqS}) + f_0 e^{2iqS}[1 + e^{iqL} + e^{2iqL} + \ldots + e^{(N-1)iqL}] + f_1 e^{3iqS} e^{(N-1)iqL}(1 + e^{iqS}) \quad (1)$$

where f_1 and f_0 are, respectively, the scattering amplitudes from the protein/water and the chitin individual sub-layers. Correspondingly, the diffraction intensity, $I(q) = F^*(q) \cdot F(q)$, is:

$$I(q) = |F|^2 = \left\{ f_0 \frac{\sin\left(\frac{NqL}{2}\right)}{\sin\left(\frac{qL}{2}\right)} + 4 f_1 \cos\left(\frac{qS}{2}\right) \cdot \cos\left[\frac{3}{2}qS + \frac{1}{2}(N-1)qL\right] \right\}^2 \quad (2)$$

In this model, the diffraction profile for the chitin crystal that contains N chains only (without protein/water coat), is then expressed, as:

$$I_1(q) = \left[f_0 \frac{\sin\left(\frac{NqL}{2}\right)}{\sin\left(\frac{qL}{2}\right)} \right]^2 \quad (3)$$

In order to qualitatively illustrate the re-distribution of chitin diffraction intensity caused by the modulated protein electron density, we calculate two diffraction profiles with the same b value as in pure chitin (i.e. $b = 1.89$ nm) (Minke and Blackwell, 1978; Sikorski et al., 2009), and $N = 4$ using Eqs. (2) and (3). When the protein sub-layers, separated by spacing $S = 1.13$ nm, are added, the main peak is substantially shifted to lower q-value (Fig. 8B).

We assume also that the spacing S may vary in different fibrils by an amount ΔS, with probability, P, that obeys a Gaussian distribution with dispersion, σ:

$$P = \frac{1}{\sigma\sqrt{2\pi}}\exp\left(-\frac{\Delta S^2}{2\sigma^2}\right) \tag{4}$$

Increasing σ will smooth the simulated diffraction profiles. The next step is averaging Eq. (2) using the Gaussian function (4). For that we use an auxiliary expression (see e.g. Zolotoyabko, 2014):

$$\int_{-\infty}^{\infty} P(\Delta S)\cdot e^{ikq\Delta S}\Delta S = \exp\left[-\frac{\sigma^2(kq)^2}{2}\right] \tag{5}$$

By the aid of Eq. (5), we find:

$$I_{av} = f_0^2(A_1 + A_2 + A_3) \tag{6}$$

with

$$A_1 = \left[\frac{\sin\left(\frac{NqL}{2}\right)}{\sin\left(\frac{qL}{2}\right)}\right]^2 \tag{7}$$

$$A_2 = 4\eta\frac{\sin\left(\frac{NqL}{2}\right)}{\sin\left(\frac{qL}{2}\right)}\left\{e^{-2\sigma^2q^2}\cdot\cos\left[2qS + \frac{(N-1)qL}{2}\right] + \exp\left(-\frac{\sigma^2q^2}{2}\right)\cdot\cos\left[qS + \frac{(N-1)qL}{2}\right]\right\} \tag{8}$$

$$A_3 = 4\eta^2\left\{1 + \exp\left(-\frac{\sigma^2q^2}{2}\right)\cdot\cos(qS) + \exp\left(-\frac{9\sigma^2q^2}{2}\right)\cdot\cos[3qS + (N-1)qL] + \frac{1}{2}e^{-2\sigma^2q^2}\cdot\cos[2qS + (N-1)qL] + \frac{1}{2}\exp(-8\sigma^2q^2)\cdot\cos[4qS + (N-1)qL]\right\} \tag{9}$$

Expressions (6–9) were used to fit the experimental diffraction profiles taken from pristine and processed tendon samples and to extract the modulation periods, S, and their dispersions, σ.

As an example, in Fig. 8C we show the measured (020) profile (dots) taken from dry intact sample superimposed with the calculated profile for $N = 3$, $b = 2L = 1.89$ nm, $S = 1.09$ nm, $\sigma = 0.19$nm (17% of S). For an intact wet sample, using the same N- and b-values, we find $S = 1.13$ nm and $\sigma = 0.16$nm (14% of S). Note that the S-value for the wet sample is slightly larger than that for the dry sample, suggesting a swelling of the protein layers in the presence of water, whereas the dispersion, σ, is smaller. This is in agreement with the general statement that "water brings more order" to crystalline/polymer systems (Duer and Veis, 2013; Dorvee and Veis, 2013; Wang et al., 2013), which is supposedly because water introduces a more homogeneous charge distribution at the interfaces (Agee et al., 2015). It is worth mentioning, that protein spacings in the range of 0.9–1.1 nm in orthogonal direction to the intra-sheet β-sheet spacing ($d = 4.5$–4.7 nm) are found in amyloid structures and are assigned to inter-sheet stacking of β-sheets (Jahn et al., 2010), giving rise to the possibility of a layered arrangement of the proteins surrounding the chitin crystals.

Interestingly, a small ($\Delta q/q \approx 1.5\%$), but clear shift of the (020) diffraction peak is observed even in protein-free wet samples, as extracted from the comparison between experimental diffraction profiles taken from wet and dry bleached samples (Fig. 7). It is noteworthy that substantial lattice swelling in the presence of water is well known for the monoclinic β-chitin, for which large actual differences (up to $\Delta b/b \approx 25\%$) between lattice parameters in the hydrated and the anhydrous forms along the b-axis have been reported (Kobayashi et al., 2010). The chitin chains in β-chitin are packed in a parallel arrangement, as opposed to the antiparallel arrangement in α-chitin. Structural studies (Nishiyama et al., 2011) suggested that β-chitin forms molecular sheets in the ac-plane by hydrophobic forces of glucopyranoside rings and intermolecular hydrogen bonds. These sheets are stacked in the b-direction via hydrophobic forces with no hydrogen bonding between the sheets along the b-direction. When β-chitin crystals swell in water, the molecular sheets remain intact but move apart allowing the intercalation of water molecules. However, it is widely accepted that this mechanism does not apply to α-chitin because the anti-parallel chain arrangement results in hydrogen bonds between the molecular sheets (Minke and Blackwell, 1978). We therefore assume that the observed shift in the (020) diffraction peak position is due to the modulation of the water electron density in close proximity to the chitin (010) surface plane, as in the case of proteins. Applying the same expressions (6)–(9), we were able to fit the experimental data using the fitted parameters values $N = 8$, $S = 0.27$ nm, and $\sigma = 0.08$nm (30% of S), keeping $b = 1.89$ nm (as in pure chitin).

The extracted modulation period, $S = 0.27$ nm, is much smaller than the protein modulation period ($S \approx 1.1$ nm). However, it is only a little smaller than the mean distance between molecules in liquid water, about 0.29 nm (Kobayashi et al., 2010; Fletcher, 1971), as can be expected for less mobile water molecules near the water/chitin interfaces. It is also noteworthy that in the case of water, the electron density modulation fluctuates more from one fibril to another, as revealed by the nearly twofold higher ratio, σ/S, as compared to the protein modulation.

In addition, we find a considerable increase of parameter N in deproteinized (bleached) sample ($N = 8$) as compared with that in intact samples ($N = 3$). This result is in accordance with the observed narrowing of diffraction peaks upon deproteinization (see Figs. 3 and 7) and confirms the idea that the tiny chitin crystals coalesce after protein removal.

Based on this analysis, we conclude that the large shifts of the (020) peak positions observed in intact samples, as compared to pure chitin, is an X-ray interference effect caused by the electron density modulation in the surrounding protein coat and water. We suggest that previously reported relative elongations, $\Delta b/b$, for other chitin-based structures (Erko et al., 2013) are of the same nature. The fact that other reflections are not influenced by such an interference effect implies either that the modulation mentioned is mainly along the b-axis or that the number of chitin unit cells is much larger along other directions in space and, hence, the contribution of a few modulated protein/water sub-layers to the diffraction profile is insignificant. In our case, most probably both factors act in unison.

The high degree of order within the protein matrix is also evidenced by the fact that the protein trace is clearly visible in the X-ray diffraction pattern (see Fig. 2). The β-sheet signature in the X-ray diffraction pattern implies that the direction orthogonal to the β-strand long axis is slightly inclined with respect to the chitin c-axis. Previous models of protein/chitin interactions in the arthropod cuticle, suggested that the β-strands in the β-sheet motif are arranged parallel to the c-axis, whereas in our case the strands

are tilted. The different arrangements may result from the presence of dissimilar proteins in each system, as expected for different phylogenic groups (i.e. spiders vs. insects). In addition, we have investigated different cuticular structures (tendon vs. ovipositor). Such variability in chitin-protein arrangements may be related to the occurrence of a rich family of chitin-binding cuticular proteins and the variability observed within the chitin-binding domains (Willis, 1999; Cornman et al., 2008). Our results are compatible with structural predictions of chitin-binding proteins containing the R&R consensus sequence, which suggest a possible arrangement of the protein β-strands perpendicular to the chitin chains long axis (Iconomidou et al., 2005). Certainly, additional work is needed in order to fully address this issue.

4. Conclusions

Using synchrotron X-ray diffraction we measured lattice parameters of the orthorhombic α-chitin crystals in the spider's tarsal tendon in intact samples and after deproteinization and dehydration. With the notable exception of the (020)-reflection, lattice parameters extracted from the set of the available intense reflections show that the α-chitin unit cell barely changes following processing. In contrast, when analyzing the (020) diffraction profiles, we find large shifts in peak position in the wet and dry intact samples, leading to an apparent increase in b lattice parameter ($\Delta b/b \approx 9$ and 6.5%, respectively), as compared to pure chitin (i.e. fully deproteinized and dried). Note, that a rather small, but clear peak shift ($\Delta b/b \approx 1.5\%$) is also observed in wet samples after complete deproteinization.

In order to explain these findings, we developed an X-ray diffraction model, which takes into account the coherent X-ray scattering not only from tiny chitin crystallites, but also from the modulated electron density along the b-axis in the protein/water layers surrounding them. In the case of proteins, the modulation period is about $S \approx 1.1$ nm, and we suggest two sub-layers of stacked β-sheets (most probably). For pure water (with no proteins), the modulation length is $S \approx 0.27$ nm, which is slightly smaller than the mean distance between molecules in liquid water.

Taken together, these findings point toward strong protein/-chitin and water/chitin interactions, which evolve over characteristic distances of about $2S \approx 2$ nm for proteins and $2S \approx 0.5$ nm for water. At present, the functional role of robust protein/chitin interaction in the cuticle is not completely clear. At least from the materials engineering point of view, a strong fiber–matrix bonding at interfaces will lead to more efficient load transfer from the rather compliant matrix to the stiff load-bearing fibers. Weak interfaces, on the other hand, facilitate component delamination, thereby increasing the risk of a catastrophic failure. In addition, the proteins are expected to play a pivotal role in cuticle formation, possibly taking part in shaping the chitin nano-crystals and controlling their size. A deeper understanding of how this sophisticated processing is achieved in nature may contribute to the design and synthesis of novel functional materials.

Acknowledgements

We thank Birgit Schonert for help with sample preparation, Stefan Siegel and Chenghao Li for assistance during the measurements at BESSY II. We thank HZB for the allocation of synchrotron radiation beam time. Special thanks to Prof. Leeor Kronik and to Ido Azuri for invaluable discussions and for critically reviewing the manuscript, and to Matthew J. Harrington for critical reading and editing of the manuscript. One of us (B. B.-O.) acknowledges the generous support from the Minerva Foundation, whereas E. Z. thanks the Shore Research Fund in Advanced Composites (Technion) for partial financial support.

References

Agee, K.A., Prakki, A., Abu-Haimed, T., Naguib, G.H., Nawareg, M.A., Tezvergil-Mutluay, A., Scheffel, D.L.S., Chen, C., Jang, S.S., Hwang, H., Brackett, M., Grégoire, G., Tay, F.R., Breschi, L., Pashley, D.H., 2015. Water distribution in dentin matrices: bound vs. unbound water. Dental Mater. 31, 205–216.

Atkins, E., 1985. Conformations in polysaccharides and complex carbohydrates. J. Biosci. 8, 375–387.

Barth, F.G., 1973. Microfiber reinforcement of an arthropod cuticle. Laminated composite material in biology. Cell Tissue Res. 144, 409–433.

Barth, F.G., 2002. A Spider's World Senses and Behavior. Springer-Verlag, Heidelberg, New York, Berlin, pp. 394.

Berman, A., Addadi, L., Weiner, S., 1988. Interactions of sea-urchin skeleton macromolecules with growing calcite crystals: a study of intracrystalline proteins. Nature 331, 546–548.

Berman, A., Addadi, L., Kvick, Å., Leiserowitz, L., Nelson, M., Weiner, S., 1990. Intercalation of sea urchin proteins in calcite: study of a crystalline composite material. Science 250, 664–667.

Blackwell, J., Weih, M.A., 1980. Structure of chitin-protein complexes: ovipositor of the ichneumon fly *Megarhyssa*. J. Mol. Biol. 137, 49–60.

Carlström, D.J., 1987. The crystal structure of alpha-chitin (poly-N-acetyl-D-glucosamine). Biophys. Biochem. Cytol. 3, 669–683.

Cheol Min, L., Eun-Min, C., Sung Ik, Y., Erdene-Ochir, G., Jehoon, J., Kwang-Hwi, C., 2013. Raman spectroscopy and density functional theory calculations of β-glucans and chitins in fungal cell walls. Bull. Korean Chem. Soc. 34, 943–945.

Cornman, R.S., Togawa, T., Dunn, W.A., He, N., Emmons, A.C., Willis, J.H., 2008. Annotation and analysis of a large cuticular protein family with the R&R consensus in *Anopheles gambiae*. BMC Genomics 9, 22–38.

Dorvee, J.R., Veis, A., 2013. Water in the formation of biogenic minerals: peeling away the hydration layers. J. Struct. Biol. 183, 278–303.

Duer, M., Veis, A., 2013. Water brings order. Nature Mater. 12, 1081–1082.

Erko, M., Hartmann, M.A., Zlotnikov, I., Valverde Serrano, C., Fratzl, P., Politi, Y., 2013. Structural and mechanical properties of the arthropod cuticle: comparison between the fang of the spider *Cupiennius salei* and the carapace of American lobster *Homarus americanus*. J. Struct. Biol. 183, 172–179.

Fengel, D., Wegener, G., 1984. Wood: Chemistry, Ultrastructure, Reactions. De Gruyter, Berlin.

Fletcher, N.H., 1971. Structural aspects of the ice–water system. Rep. Prog. Phys. 34, 913–994.

Fossey, S.A., Kaplan, D., 1993. In silk polymers ACS symposium series. Am. Chem. Soc. 544, 23–270.

Fraenkel, G., Rudall, K.M., 1947. The structure of insect cuticles. Proc. R. Soc. London Ser. B 134, 111–143.

Geddes, A.J., Parker, K.D., Atkins, E.D.T., Beighton, E., 1968. "Cross-β" conformation in proteins. J. Mol. Biol. 32, 343–358.

Iconomidou, V.A., Chryssikos, G.D., Gionis, V., Willis, J.H., Hamodrakas, S., 2001. "Soft"-cuticle protein secondary structure as revealed by FT-Raman, ATR FT-IR and CD spectroscopy. J. Insect Biochem. Mol. Biol. 31, 877–885.

Iconomidou, V.A., Willis, J.H., Hamodrakas, S., 2005. Unique features of the structural model of 'hard' cuticle proteins: implications for chitin-protein interactions and cross-linking in cuticle. J. Insect Biochem. Mol. Biol. 35, 553–560.

Jahn, T.R., Makin, O.S., Morris, K.L., Marshall, K.E., Tian, P., Sikorski, P., Serpell, L.C., 2010. The common architecture of cross-beta amyloid. J. Mol. Biol. 395, 717–727.

Kobayashi, K., Kimura, S., Togawa, E., Wada, M., 2010. Crystal transition between hydrate and anhydrous β-chitin monitored by synchrotron X-ray fiber diffraction. Carbohydr. Polym. 79, 882–889.

Lowenstam, H.A., Weiner, S., 1989. On Biomineralization. Oxford University Press, New York.

Mann, S., 2001. Biomineralization: Principles and Concepts in Bioinorganic Materials Chemistry. Oxford University Press, New York.

Merkel, J.S., Sturtevant, J.M., Regan, L., 1999. Side chain interactions in parallel β sheets: the energetics of cross-strand pairings. Structure 7, 1333–1343.

Minke, R., Blackwell, J., 1978. The structure of α-chitin. J. Mol. Biol. 120, 167–181.

Neville, A.C., 1967. In Advances in Insect Physiology, 4. Academic Press, pp. 213–286.

Neville, A.C., 1993. Biology of Fibrous Composites: Development Beyond the Cell Membrane. Cambridge University Press, New York.

Neville, A.C., Parry, D.A., Woodhead-Galloway, J., 1976. The chitin crystallite in arthropod cuticle. J. Cell Sci. 21, 73–82.

Nishiyama, Y., Noishiki, Y., Wada, M., 2011. X-ray structure of anhydrous β-chitin at 1 Å resolution. Macromolecules 44, 950–957.

Oh, S.H., Kauffmann, Y., Scheu, C., Kaplan, W.D., 2005. Ordered liquid aluminum at the interface with sapphire. Science 310, 661–663.

Pokroy, B., Quintana, J.P., Caspi, E.N., Berner, A., Zolotoyabko, E., 2004. Anisotropic lattice distortions in biogenic aragonite. Nat. Mater. 3, 900–902.

Pokroy, B., Fitch, A.N., Zolotoyabko, E., 2006a. The microstructure of biogenic calcite: a view by high-resolution synchrotron powder diffraction. Adv. Mater. 18, 2363–2368.

Pokroy, B., Fitch, A.N., Marin, F., Kapon, M., Adir, N., Zolotoyabko, E., 2006b. Anisotropic lattice distortions in biogenic calcite induced by intra-crystalline organic molecules. J. Struct. Biol. 155, 96–103.
Rebers, J.E., Willis, J.H., 2001. A conserved domain in arthropod cuticular proteins binds chitin. Insect Biochem. Mol. Biol. 31, 1083–1093.
Rudall, K.M., 1963. In Advances in Insect Physiology, 1. Academic Press, pp. 257–313.
Sikorski, P., Hori, R., Wada, M., 2009. Revisit of alpha-chitin crystal structure using high resolution X-ray diffraction data. Biomacromolecules 10, 1100–1105.
Speck, J., Barth, F., 1982. Vibration sensitivity of pretarsal slit sensilla in the spider leg. J. Comp. Physiol. 148, 187–194.
Suetake, T., Tsuda, S., Kawabata, S., Miura, K., Iwanaga, S., Hikichi, K., Nitta, K., Kawano, K., 2000. Chitin-binding proteins in invertebrates and plants comprise a common chitin-binding structural motif. J. Biol. Chem. 275, 17929–17932.
Sunde, M., Serpell, L.C., Bartlam, M., Fraser, P.E., Pepys, M.B., Blake, C.C., 1997. Common core structure of amyloid fibrils by synchrotron X-ray diffraction. J. Mol. Biol. 273, 729–739.
Valluzzi, R., Jin, H.-J., 2004. X-ray evidence for a "Super"-secondary structure in silk fibers. Biomacromolecules 5, 696–703.
Vincent, J.F.V., Wegst, U.G.K., 2004. Design and mechanical properties of insect cuticle. Arthropod Struct. Dev. 33, 187–199.
Wang, Y., Von Euw, S., Fernandes, F.M., Cassaigno, S., Selmane, M., Laurent, G., Pehau-Arnaudet, G., Coelho, C., Bonhomme-Coury, L., Giraud-Guille, M.-M., Babonneau, F., Azaïs, T., Nassif, N., 2013. Water-mediated structuring of bone apatite. Nat. Mater. 12, 1144–1153.
Weiner, S., Wagner, H.D., 1998. The material bone: structure-mechanical function relations. Annu. Rev. Mater. Sci. 28, 271–298.
Willis, J.H., 1999. Cuticular proteins in insects and crustaceans. Integr. Comp. Biol. 39, 600–609.
Zhang, K., Geissler, A., Fischer, S., Brendler, E., Bäucker, E., 2012. Solid-state spectroscopic characterization of α-chitins deacetylated in homogeneous solutions. J. Phys. Chem. B 116, 4584–4592.
Zolotoyabko, E., 2014. Basic Concepts of X-Ray Diffraction. Wiley-VCH, Weinheim.
Zolotoyabko, E., Pokroy, B., 2007. Biomineralization of calcium carbonate: structural aspects. CrystEngComm 9, 1156–1161.